Intrinsic Transverse Motion of the Pion's Valence Quarks

Chao Shi and Ian C. Cloët

Phys. Rev. Lett. **122**, 082301 — Published 1 March 2019

DOI: 10.1103/PhysRevLett.122.082301

Intrinsic Transverse Motion of the Pion's Valence Quarks

Chao Shi[1] and Ian C. Cloët[1]

[1]*Physics Division, Argonne National Laboratory, Argonne, IL 60439 USA*

Starting with the solution to the Bethe-Salpeter equation for the pion, in a beyond rainbow-ladder truncation to QCD's Dyson-Schwinger equations (DSEs), we determine the pion's $l_z = 0$ and $|l_z| = 1$ leading Fock-state light-front wave functions (LFWFs) [labeled by $\psi_{l_z}(x, \boldsymbol{k}_T^2)$]. The leading-twist time-reversal even transverse momentum dependent parton distribution function (TMD) of the pion is then directly obtained using these LFWFs. A key characteristic of the LFWFs, which is driven by dynamical chiral symmetry breaking, is that at typical hadronic scales they are broad functions in the light-cone momentum fraction x. The LFWFs have a non-trivial $(x, \boldsymbol{k}_T^2)$ dependence and in general do not factorize into separate functions of each variable. For $\boldsymbol{k}_T^2 \lesssim 1\,\text{GeV}^2$ the $\boldsymbol{k}_T^2$ dependence of the LFWFs is well described by a Gaussian, however for $\boldsymbol{k}_T^2 \gtrsim 10\,\text{GeV}^2$ these LFWFs behave as $\psi_0 \propto x(1-x)/\boldsymbol{k}_T^2$ and $\psi_1 \propto x(1-x)/\boldsymbol{k}_T^4$, and therefore exhibit the power-law behavior predicted by perturbative QCD. The pion's TMD naturally inherits many features from the LFWFs. The TMD evolution of our result is studied using both the b^* and ζ prescriptions which allows a qualitative comparison with Drell-Yan data.

Light-front quantization and the associated light-front wave functions (LFWFs) provide a powerful framework with which to study quantum chromodynamics (QCD) [1, 2]. Hadron observables such as form factors, parton distribution functions (PDFs), and their multi-dimensional counterparts such as generalized and transverse momentum dependent PDFs (TMDs) can each be expressed as overlaps of LFWFs [3, 4]. Therefore LFWFs allow features of apparent disparate hadron observables to be straightforwardly related to underlying quark-gluon dynamics in a QCD Fock-state expansion. In principle, the LFWFs can be computed by diagonalizing the light-cone QCD Hamiltonian operator, using methods such as discretized light-cone quantization [5] and basis light-front quantization [6, 7], or by effective interaction methods such as holographic QCD [8].

Another approach used to study QCD, which is explicitly Poincaré-covariant, is provided by judicious truncations to QCD's Dyson-Schwinger equations (DSEs) [9–11]. In the DSE framework hadron states are obtained as solutions to Poincaré-covariant bound-state equations such as the Bethe-Salpeter and Faddeev equations [12, 13]. Insights into numerous aspects of hadron structure have been revealed using the DSEs [11, 14], with particular success in understanding the pion as both a relativistic bound-state of a dressed quark and dressed antiquark, and the Goldstone mode associated with dynamical chiral symmetry breaking (DCSB) in QCD [11, 15–17]. DSE solutions to the Bethe-Salpeter equation (BSE), which naturally contain an infinite number of Fock-states and can therefore encapsulate key emergent QCD phenomena such as DCSB and quark confinement, provide an excellent starting point from which to extract the pion's LFWFs. In particular, the properties of the LFWFs can then be clearly connected to underlying quark-gluon dynamics as expressed in the dressing functions for propagators and vertices. The calculation of the pion's leading Fock-state LFWFs using the DSEs, and the application of these LFWFs to a calculation of the pion's leading-twist time-reversal even TMD is the focus of this paper. Such a study is timely because the proposed electron-ion collider [18] could study the partonic structure of the pion and kaon [19].

In the light-front formalism a hadron state can be expressed as the superposition of Fock-state components classified by their orbital angular momentum projection l_z [20]. For the pion the minimal ($|\bar{q}q\rangle$) Fock-state configuration reads [20, 21] $|\pi^+(p)\rangle = |\pi^+(p)\rangle_{l_z=0} + |\pi^+(p)\rangle_{|l_z|=1}$. The non-perturbative content of each state is contained in the LFWFs [4], labeled by $\psi_0(x, \boldsymbol{k}_T^2)$ for $l_z = 0$ and $\psi_1(x, \boldsymbol{k}_T^2)$ for $|l_z| = 1$, where $\boldsymbol{k}_T$ is the transverse momentum of the quark and $x = \frac{k^+}{p^+}$ is its light-cone momentum fraction.

The pion's minimal Fock-state LFWFs can be obtained from the pion's Bethe-Salpeter wave function via [22]

$$\psi_0(x, \boldsymbol{k}_T^2) = \sqrt{3}\, i \int \frac{dk^+ dk^-}{2\,\pi} \times \text{Tr}_D\left[\gamma^+ \gamma_5 \chi(k,p)\right] \delta\left(k^+ - x\,p^+\right), \quad (1)$$

$$\psi_1(x, \boldsymbol{k}_T^2) = -\sqrt{3}\, i \int \frac{dk^+ dk^-}{2\,\pi} \frac{1}{\boldsymbol{k}_T^2} \times \text{Tr}_D\left[i\sigma_{+i}\, k_T^i\, \gamma_5\, \chi(k,p)\right] \delta\left(k^+ - x\,p^+\right). \quad (2)$$

The Bethe-Salpeter wave function for the π^+ is defined by the quark-antiquark correlator $\chi(k,p) = \int d^4z\; e^{-ik\cdot z}\, \langle 0|\mathcal{T} u(z)\, \bar{d}(0)|\pi^+(p)\rangle$ [23, 24] and can be expressed as $\chi(k,p) = S(k)\,\Gamma(k,p)\,S(k-p)$, where $S(k)$ is the dressed quark propagator and $\Gamma(k,p)$ the pion's homogeneous Bethe-Salpeter amplitude [9, 25].

The BSE, whose solution gives the wave function $\chi(k,p)$, self-consistently sums of an infinite number of Fock components. For example, in the rainbow-ladder trunction of QCD's DSEs[1] $\chi(k,p)$ not only contains the minimal $|\bar{q}q\rangle$ Fock-state but also the Fock components with any number of gluons: $|\bar{q}qg\ldots\rangle$. In the DSEs it is this sum over the infinite tower of gluons that gives raise to emergent phenomena such as DCSB and confinement, which is then encoded in

[1] In this work will use a beyond rainbow-ladder trunction to the DSEs called the DCSB-improved truncation.

$\chi(k,p)$. A key advantage of projecting out the LFWFs from the Bethe-Salpeter wave function, as done in Eqs. (1) and (2) for the minimal Fock-state, is that effects from these emergent phenomena are encoded in all LFWFs. In addition, an analogous procedure to that defined in Eqs (1) and (2) can be used to obtain higher Fock-state LFWFs, such as those that correspond to $|\bar{q}qg\rangle$ states, via project from $\chi(k,p)$ and elements of its Bethe-Salpeter kernel. Since $\chi(k,p)$ is the same for each LFWF projection, such a method leaves the LFWFs corresponding to other Fock components unchanged. Therefore, this method in principle allows for the self-consistent and systematic solution of the tower of LFWFs, allowing the importance of higher Fock components in hadron structure and reactions to be systematically studied.

The pion's Bethe-Salpeter wave function can be calculated within the DSE framework [26], via a self-consistent solution to the quark gap equation for $S(k)$, and the homogeneous BSE which gives $\Gamma(k,p)$. To solve these equations a truncation to the interaction kernel must be employed, such that the key symmetries of QCD are maintained. In the context of the pion the axial-vector Ward-Takahashi identity plays an important role [27], as it is an expression of chiral symmetry and its dynamical breaking [28]. The simplest symmetry-preserving DSE truncation is rainbow-ladder [27, 29, 30]. Here we use a modern extension known as the DCSB-improved truncation, that includes an anomalous chromomagnetic moment term in the dressed quark-gluon vertex [31], which in the chiral limit can only exist through DCSB. This truncation provides the most realistic description of the pion currently available within the DSEs formalism [11].

The DSEs are formulated in Euclidean space and therefore a direct calculation of light-cone dominated quantities is challenging. However, an arbitrary $\boldsymbol{k}_T^2$-dependent moment of the pion's LFWFs, defined by $\langle x^m\rangle_{l_z}(\boldsymbol{k}_T^2) = \int_0^1 dx\, x^m\, \psi_{l_z}(x,\boldsymbol{k}_T^2)$ can be directly calculated, and the LFWFs for the pion can then be accurately reconstructed from these moments. In fact, an arbitrary moment of a LFWF can be expressed as $\langle x^m\rangle_{l_z}(\boldsymbol{k}_T^2) = \int_0^1 d\alpha\, \alpha^m \int d\beta d\gamma\, f_{l_z}(\alpha,\boldsymbol{k}_T^2,\beta,\gamma)$ and therefore the LFWF is identified as $\psi_{l_z}(x,\boldsymbol{k}_T^2) = \int d\beta d\gamma\, f_{l_z}(x,\boldsymbol{k}_T^2,\beta,\gamma)$ [22, 32].

To aid the calculation of the moments we use an accurate parametrization of numerical solutions to the gap and BSEs in the DCSB-improved truncation to the DSEs [17, 31]. The dressed quark propagator is parametrized with two pairs of complex conjugate poles [33, 34]: $S(k) = \sum_{i=1}^{2}[z_i/(i\not{k} + m_i) + z_i^*/(i\not{k} + m_i^*)]$ where z_i and m_i are complex numbers determined by fitting to the numerical DSE solution to the gap equation. The general Bethe-Salpeter amplitude for the pion reads [15, 25]: $\Gamma_\pi(k,p) = \gamma_5\big[iE(k,p) + \not{p}\,F(k,p) + \not{k}\,G(k,p) + [\not{p},\not{q}]\,H(k,p)\big]$. We retain the dominant E and F amplitudes, and further details about the model are provided in the supplementary material and Refs. [17, 31].

Results for the pion's minimal Fock-state LFWFs are illustrated in Fig. 1, where the LFWFs satisfy the normalization condition $\int_0^1 dx \int \frac{d^2\boldsymbol{k}_T}{(2\pi)^3}\Big[|\psi_0(x,\boldsymbol{k}_T^2)|^2 + \boldsymbol{k}_T^2|\psi_1(x,\boldsymbol{k}_T^2)|^2\Big] = 1$. For each x, the $\boldsymbol{k}_T^2$ dependence of the LFWFs exhibits a Gaussian-like behavior for $\boldsymbol{k}_T^2 \lesssim 1\,\text{GeV}^2$, a transition then begins to occur and for $\boldsymbol{k}_T^2 \gtrsim 10\,\text{GeV}^2$ the LFWFs become $\psi_0(x,\boldsymbol{k}_T^2) \propto x(1-x)/\boldsymbol{k}_T^2$ and $\psi_1(x,\boldsymbol{k}_T^2) \propto x(1-x)/\boldsymbol{k}_T^4$, which matches the power-law behavior predicted by perturbative QCD [21]. The factorization between x and $\boldsymbol{k}_T^2$ is only seen in the scaling regime, where the onset reflects the ultraviolet behavior of the Bethe-Salpeter dressing functions which behave as $E, F \sim 1/k^2$ for $k^2 \gtrsim 10\,\text{GeV}^2$ [27] (k is the relative momentum).

An important characteristic of our LFWF results, when viewed as a function of x, is that they are broad with significant support near the $x = 0, 1$ end-points for $\boldsymbol{k}_T^2 \lesssim 1\,\text{GeV}^2$. As discussed in Ref. [17] in the context of the pion's parton distribution amplitude (PDA), this broadening of the LFWFs is directly linked to DCSB, however this effect diminishes for $\boldsymbol{k}_T^2 \gg \Lambda_{\text{QCD}}^2$ where the x-dependence of both LFWFs is the same as the asymptotic pion PDA [35]. This manifestation of DCSB on the light-front will therefore have a material impact on observables sensitive to the LFWFs in the region $\boldsymbol{k}_T^2 \lesssim 1\,\text{GeV}^2$. The $l_z = 0$ LFWF is concave in x with a maximum at $x = 1/2$ for all $\boldsymbol{k}_T^2$, whereas orbital angular momentum effects causes the $|l_z| = 1$ LFWF to have a slight *double-humped* structure for quark transverse momentum in the range $0.5 \lesssim \boldsymbol{k}_T^2 \lesssim 5\,\text{GeV}^2$, which is evident in Fig. 1. Near the $x = 0, 1$ end-points we find that each LFWF behaves linearly as a function of x, that is, as $x \to 1$ we have $\psi_{l_z}(x,\boldsymbol{k}_T^2) \sim 1 - x$, with analogous results near $x \to 0$ because $\psi_{l_z}(x,\boldsymbol{k}_T^2) = \psi_{l_z}(1-x,\boldsymbol{k}_T^2)$. This linear behavior in $1 - x$ is a necessary property of the LFWFs if they are to give a pion TMD or PDF behaving as $f(x) \to (1-x)^2$ near $x = 1$, as predicted by perturbative QCD [36–38].

With the pion's LFWFs in hand it straightforward to determine properties of the pion. We focus on the pion's leading-twist time-reversal even TMD which in terms of the pion's minimal Fock-state LFWFs reads [4]

$$f_\pi^{\mu_0}(x,\boldsymbol{k}_T^2) = \left[|\psi_0^{\mu_0}(x,\boldsymbol{k}_T^2)|^2 + \boldsymbol{k}_T^2|\psi_1^{\mu_0}(x,\boldsymbol{k}_T^2)|^2\right]/(2\pi)^3, \quad (3)$$

where we have made explicit the renormalization scale dependence. At the inital renormalization scale (μ_0) the pion's valence quark PDF is related to the TMD by $f_\pi^{\mu_0}(x) = \int d^2\boldsymbol{k}_T\, f_\pi^{\mu_0}(x,\boldsymbol{k}_T^2)$, where the normalization condition for the LFWFs guarantees baryon number conservation.[2] The symmetry under $x \to 1-x$ of the LFWFs ensures $\langle x\rangle^{\mu_0} = 0.5$ and therefore the two valence quarks carry all the light-cone momentum. This is to be expected because only the leading Fock-state LFWFs are used to determine the pion's PDF. By associating the renormalization scale with the resolving scale ($\mu_0^2 = Q^2$), it is clear that as μ_0^2 gets larger

[2] This naive relation between the TMD and PDF is only valid at the model scale, since evolution to a scale $\mu \neq \mu_0$ breaks this correspondence.

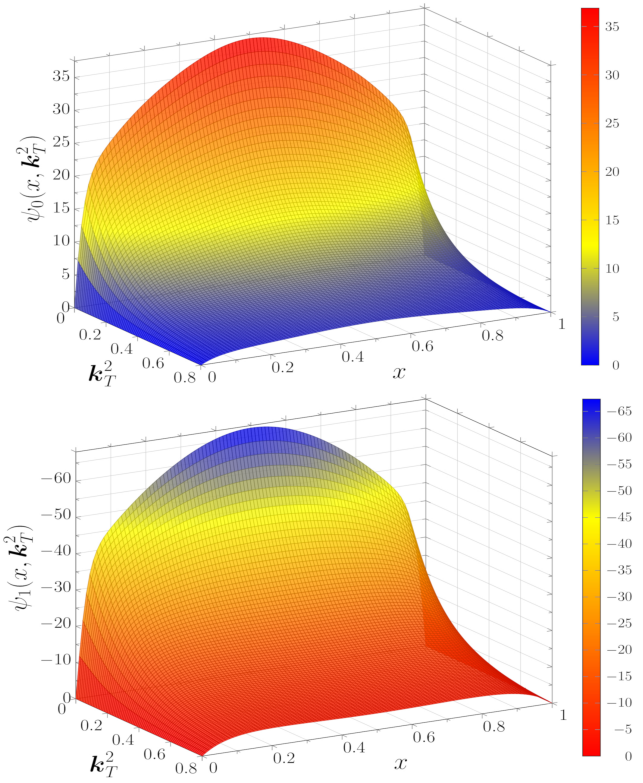

Figure 1. *Upper panel:* DSE result for the pion's $l_z = 0$ minimal Fock-state LFWF. *Lower panel:* Analogous result for the pion's $|l_z| = 1$ minimal Fock-state LFWF. The LFWFs are given in units of GeV^{-2} and $\boldsymbol{k}_T^2$ in GeV^2.

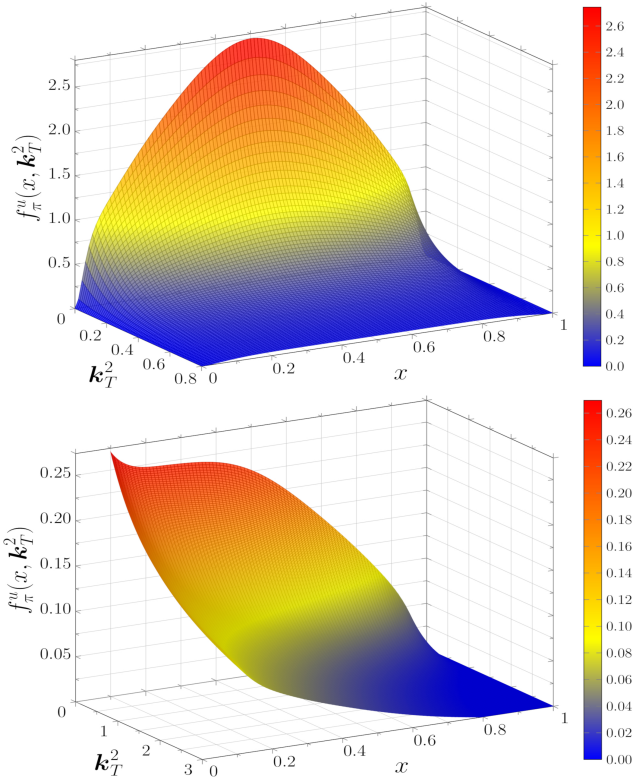

Figure 2. *Upper panel:* DSE result for the time-reversal even u-quark TMD of the pion, $f_\pi^u(x, \boldsymbol{k}_T^2)$, at the model scale of $\mu_0^2 = 0.52\,\text{GeV}^2$. *Lower panel:* Analogous result evolved to a scale of $\mu = 6\,\text{GeV}$ using TMD evolution with the b^* prescription and $g_2 = 0.09\,\text{GeV}$ [42]. The TMDs are given in units of GeV^{-2} and $\boldsymbol{k}_T^2$ in GeV^2.

higher Fock-states play an increasingly important role, and therefore the minimal Fock-state contributions calculated here can only dominate at a low resolving scale [20]. The renormalization scale associated with our DSE calculation is determined such that the momentum fraction carried by the valence quarks agrees with results from a πN Drell-Yan analysis: $2\,\langle x\rangle_v = 0.47(2)$ [39, 40] at a scale of $Q^2 = 4\,\text{GeV}^2$. NLO DGLAP [41] gives $\mu_0 = 0.52\,\text{GeV}$.

Our DSE result for the time-reversal even u-quark TMD in the π^+, obtained from the LFWFs using Eq. (3), is given in the upper panel of Fig. 2. These calculations are performed with equal current quark masses. Several features of the LFWFs are immediately reflected in the TMD at the hadronic scale, notably in the limit $x \to 1$ the TMD behaves as $f_\pi^u(x, \boldsymbol{k}_T^2) \propto (1-x)^2$ for all $\boldsymbol{k}_T^2$, in agreement with perturbative QCD [38]. As $\boldsymbol{k}_T^2$ becomes large our TMDs exhibits two scaling regimes, for $\boldsymbol{k}_T^2 \gtrsim 10\,\text{GeV}^2$ the pion's TMD has a power-law behavior of $f_\pi^u(x, \boldsymbol{k}_T^2) \propto 1/\boldsymbol{k}_T^6$ which reflects the dominance of $\psi_1(x, \boldsymbol{k}_T^2)$ in this region. The $l_z = 0$ LFWF only begins to dominate the TMD for $\boldsymbol{k}_T^2 \gtrsim 100\,\text{GeV}^2$, where we obtain our asymptotic result for the TMD: $f_\pi^u(x, \boldsymbol{k}_T^2) \propto x^2(1-x)^2/\boldsymbol{k}_T^4$. At the low hadron scale our DSE result for the pion's TMD is a broad unimodal function of x for $\boldsymbol{k}_T^2 \lesssim 0.7\,\text{GeV}^2$, however in the range $0.7 \lesssim \boldsymbol{k}_T^2 \lesssim 5\,\text{GeV}^2$ the slight *double-humped* feature of $\psi_1(x, \boldsymbol{k}_T^2)$ manifests in the TMD. This double-humped structure is seen more prominently in some light-front constituent quark [4] and holographic QCD models [43]. Because our TMD result scales as $f_\pi^u(x, \boldsymbol{k}_T^2) \propto 1/\boldsymbol{k}_T^4$, our result for the average $\boldsymbol{k}_T^2$ of the TMD is logarithmically divergent if $\langle \boldsymbol{k}_T^2 \rangle$ is defined in the usual way [44]. We therefore study two methods: fitting a Gaussian ansatz to our TMD for $\boldsymbol{k}_T^2 < 1\,\text{GeV}^2$ gives $\langle \boldsymbol{k}_T^2 \rangle = 0.16\,\text{GeV}^2$, and using the Bessel-weighted definition of Ref. [45] with $\boldsymbol{b}_T = 0.3\,\text{fm}$ gives $\langle \boldsymbol{k}_T^2 \rangle = 0.19\,\text{GeV}^2$ at the model scale. Therefore, the average transverse momentum is typical of the infrared scale of the dressed quark mass.

To compare our results with data it is essential to perform TMD evolution [46, 47]. TMD evolution is governed by renormalization group equations involving two scales, μ and ζ, which are set to the hard scale $\mu^2 = \zeta = Q^2$ [48]. The lower panel of Fig. 2 presents our pion TMD result evolved to a scale of $\mu = 6\,\text{GeV}$, which is a typical scale associated with the E-615 pion-induced Drell-Yan experiment [49]. The illustrated result uses the b^*-prescription [50], where we follow closely the implementation of Refs. [42, 43], and to parameterize the non-perturbative behavior of the ζ evolution kernel [47] we choose $g_2 = 0.09$ in accordance with Ref. [43]. The effect of the TMD evolution is dramatic,

shifting significant strength to small x and large $\boldsymbol{k}_T^2$, with a factor of 10 reduction in the magnitude of the TMD near $x \sim 1/2$, $\boldsymbol{k}_T^2 \sim 0$ compared to the model scale result. For the evolved TMD we find $\langle \boldsymbol{k}_T^2 \rangle = 0.69\,\mathrm{GeV}^2$ using the Gaussian fit method, and the Bessel-weighted definition with $\boldsymbol{b}_T = 0.3\,\mathrm{fm}$ gives $\langle \boldsymbol{k}_T^2 \rangle = 0.49\,\mathrm{GeV}^2$.

To attempt a quantitative comparison of our results with data we study the transverse momentum dependence characterized by a fitting function $P(x_F, \boldsymbol{p}_T; m_{\mu\mu})$ measured in the E-615 pion-induced Drell-Yan experiment on a tungsten target [49, 51, 52]. This function is defined by

$$\frac{d^3\sigma}{dx_\pi dx_N d\boldsymbol{p}_T} = \frac{d^2\sigma}{dx_\pi dx_N} P(x_F, \boldsymbol{p}_T; m_{\mu\mu}), \tag{4}$$

where x_π, x_N are the Bjorken scaling variables of the pion and nucleon, $x_F = x_\pi - x_N$, $\boldsymbol{p}_T$ is the transverse momentum of the produced dilepton pair, and $m_{\mu\mu}^2 = s\, x_\pi x_N$ is the invariant mass-squared of the dilepton pair where $s = (p_\pi + p_N)^2$ is the center-of-mass energy squared. For the fitting function P we have the relation $P(x_F, \boldsymbol{p}_T; m_{\mu\mu})/|\boldsymbol{p}_T| \propto F_{UU}^1(x_\pi, x_N, \boldsymbol{p}_T)$, where within the TMD factorization scheme, at leading twist, and including only the W-term in the cross-section, the unpolarized Drell-Yan structure function is given by [4, 52, 53]

$$F_{UU}^1(x_\pi, x_N, \boldsymbol{p}_T) = \frac{1}{N_c} \sum_q e_q^2 \int d^2\boldsymbol{k}_T d^2\boldsymbol{\ell}_T \times \delta(\boldsymbol{p}_T - \boldsymbol{k}_T - \boldsymbol{\ell}_T)\, f_\pi^{\bar{q}}(x_\pi, \boldsymbol{k}_T^2)\, f_A^q(x_N, \boldsymbol{\ell}_T^2), \tag{5}$$

where the sum is over quark flavors $q = u, d$, and we approximate the unpolarized TMD of the tungsten target by a sum over nucleon TMDs: $f_A^q(x, \boldsymbol{\ell}_T^2) = Z/A\, f_p^q(x, \boldsymbol{\ell}_T^2) + N/A\, f_n^q(x, \boldsymbol{\ell}_T^2)$. To evaluate $F_{UU}^1(x_\pi, x_N, \boldsymbol{p}_T)$ and thereby make a qualitative comparison with data for $P(x_F, \boldsymbol{p}_T; m_{\mu\mu})$ obtained in the E-615 experiment [49] we combine our DSE results for $f_\pi^q(x_\pi, \boldsymbol{k}_T^2)$ with two sets of empirical extractions of $f_p^q(x, \boldsymbol{\ell}_T^2)$ and $f_n^q(x, \boldsymbol{\ell}_T^2)$ from Refs. [42] and [54] respectively.

Results for the fitting function $P(x_F, \boldsymbol{p}_T; m_{\mu\mu})/|\boldsymbol{p}_T|$ are presented in Fig. 3. The solid lines are empirical results from Ref. [49] for $x_F = 0, 0.25, 0.5$ where empirically $m_{\mu\mu} \simeq 6\,\mathrm{GeV}$ and $\sqrt{s} = 22\,\mathrm{GeV}$. The shaded regions in Fig. 3 are our calculated results for $\mathcal{N}\, F_{UU}^1(x_\pi, x_N, \boldsymbol{p}_T)$ for $0 \leqslant g_2 \leqslant 0.13\,\mathrm{GeV}$, where for each g_2 the normalization $\mathcal{N}$ is chosen so that this result equals $P(x_F, \boldsymbol{p}_T; m_{\mu\mu})/|\boldsymbol{p}_T|$ at $|\boldsymbol{p}_T| = 0.125\,\mathrm{GeV}$, which represents the lowest $|\boldsymbol{p}_T|$ value in the E-615 data set [55]. Since Eq. (5) only describes the W-term we restrict $|\boldsymbol{p}_T| \leqslant 0.2\, m_{\mu\mu}$ following the finding of Ref. [54]. To study the "prescription dependence" of the TMD evolution, we also present evolved TMD results using the ζ-prescription [54] as the dashed lines in Fig. 3, where we have taken $g_2 = 0$.[3] As made clear from Fig. 3

[3] The quantity g_2 is the rapidity anomalous dimension, an inherently non-perturbative parameter that is separate from the TMDs but enters the TMD evolution equations. For the TMD evolution we follow closely Ref. [42].

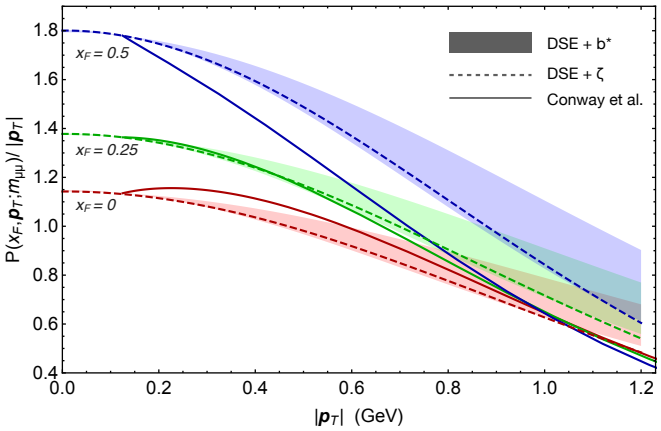

Figure 3. The solid lines are empirical results from the E-615 experiment [49] for $P(x_F, \boldsymbol{p}_T; m_{\mu\mu})/|\boldsymbol{p}_T|$ (no uncertainties are provided) and the curves in ascending order correspond to $x_F = 0, 0.25, 0.5$. The neighboring shaded bands correspond to the same x_F values, and are our results evolved using the b^*-prescription as outlined in Ref. [42], with the non-perturbative parameter g_2 in the range $0 \leqslant g_2 \leqslant 0.13$ (the lower boundary corresponds to $g_2 = 0$). The dashed lines are obtained using the ζ-prescription from Ref. [54] with $g_2 = 0$. In this prescription g_2 is much more constrained, with the small uncertainty easily contained within the existing shaded region.

the two evolution prescriptions give similar results, and our results for the fitting function P at $x_F = 0, 0.25$ are in good agreement with E-615 data. For $x_F = 0.5$ we find a discrepancy with data of around 30%, however for each x_F our results favor a small value for g_2 as suggested in Ref. [54]. Agreement with data could be improved by increasing the initial scale of the DSE calculations, which is an indication that higher Fock-states may play an important role.

Using the DCSB-improved truncation to QCD's DSEs we have determined the pion's minimal Fock-state LFWFs from the solution to the BSE, and from these LFWFs the pion's leading-twist time-reversal even TMD. The pion – as the Goldstone boson associated with DCSB in QCD – provides the ideal environment to study the impact of DCSB on hadron structure. We find that DCSB effects produce broad unimodal LFWFs and TMD, when viewed as a function of x, for small $\boldsymbol{k}_T^2$. In this regime the $\boldsymbol{k}_T^2$ dependence of the pion's LFWFs and TMD, for a given x, is well described by a Gaussian, however the x and $\boldsymbol{k}_T^2$ does not factorize. These DCSB driven effects diminish slowly as $\boldsymbol{k}_T^2$ becomes large, where for $\boldsymbol{k}_T^2 \gtrsim 10\,\mathrm{GeV}^2$ the LFWFs scale as $\psi_0 \propto x(1-x)/\boldsymbol{k}_T^2$ and $\psi_1 \propto x(1-x)/\boldsymbol{k}_T^4$ in agreement with the power-law behavior predicted by perturbative QCD. These results illustrate how a momentum tomography for the pion can shed light on hadron structure effects driven by DCSB and also help expose the transition from the non-perturbative to perturbative regimes in QCD.

CS thanks Cédric Mezrag for helpful conversations and Alexey Vladimirov for generous assistance with arTeMiDe. This work was supported by the U.S. Department of Energy, Office of Science, Office of Nuclear Physics, contract

no. DE-AC02-06CH11357; and the Laboratory Directed Research and Development (LDRD) funding from Argonne National Laboratory, project no. 2016-098-N0 and project no. 2017-058-N0.

[1] S. J. Brodsky, H.-C. Pauli, and S. S. Pinsky, Phys. Rept. **301**, 299 (1998), arXiv:hep-ph/9705477 [hep-ph].

[2] T. Heinzl, *Methods of quantization. Proceedings, 39. Internationale Universitätswochen für Kern- und Teilchenphysik, IUKT 39: Schladming, Austria, February 26-March 4, 2000*, Lect. Notes Phys. **572**, 55 (2001), arXiv:hep-th/0008096 [hep-th].

[3] S. J. Brodsky, M. Diehl, and D. S. Hwang, Nucl. Phys. **B596**, 99 (2001), arXiv:hep-ph/0009254 [hep-ph].

[4] B. Pasquini and P. Schweitzer, Phys. Rev. **D90**, 014050 (2014), arXiv:1406.2056 [hep-ph].

[5] H. C. Pauli and S. J. Brodsky, Phys. Rev. **D32**, 2001 (1985).

[6] J. P. Vary, H. Honkanen, J. Li, P. Maris, S. J. Brodsky, A. Harindranath, G. F. de Teramond, P. Sternberg, E. G. Ng, and C. Yang, Phys. Rev. **C81**, 035205 (2010), arXiv:0905.1411 [nucl-th].

[7] Y. Li, P. Maris, and J. P. Vary, Phys. Rev. **D96**, 016022 (2017), arXiv:1704.06968 [hep-ph].

[8] S. J. Brodsky, G. F. de Teramond, H. G. Dosch, and J. Erlich, Phys. Rept. **584**, 1 (2015), arXiv:1407.8131 [hep-ph].

[9] C. D. Roberts and A. G. Williams, Prog. Part. Nucl. Phys. **33**, 477 (1994), arXiv:hep-ph/9403224 [hep-ph].

[10] R. Alkofer and L. von Smekal, Phys. Rept. **353**, 281 (2001), arXiv:hep-ph/0007355 [hep-ph].

[11] I. C. Cloët and C. D. Roberts, Prog. Part. Nucl. Phys. **77**, 1 (2014), arXiv:1310.2651 [nucl-th].

[12] I. C. Cloët, G. Eichmann, B. El-Bennich, T. Klahn, and C. D. Roberts, Few Body Syst. **46**, 1 (2009), arXiv:0812.0416 [nucl-th].

[13] G. Eichmann, R. Alkofer, A. Krassnigg, and D. Nicmorus, Phys. Rev. Lett. **104**, 201601 (2010), arXiv:0912.2246 [hep-ph].

[14] G. Eichmann, H. Sanchis-Alepuz, R. Williams, R. Alkofer, and C. S. Fischer, Prog. Part. Nucl. Phys. **91**, 1 (2016), arXiv:1606.09602 [hep-ph].

[15] P. Maris, C. D. Roberts, and P. C. Tandy, Phys. Lett. **B420**, 267 (1998), arXiv:nucl-th/9707003 [nucl-th].

[16] L. Chang, I. C. Cloët, C. D. Roberts, S. M. Schmidt, and P. C. Tandy, Phys. Rev. Lett. **111**, 141802 (2013), arXiv:1307.0026 [nucl-th].

[17] L. Chang, I. C. Cloët, J. J. Cobos-Martinez, C. D. Roberts, S. M. Schmidt, and P. C. Tandy, Phys. Rev. Lett. **110**, 132001 (2013), arXiv:1301.0324 [nucl-th].

[18] The Nuclear Science Advisory Committee's October 2015 Long Range Plan for Nuclear Science, *Reaching for the Horizon*.

[19] Workshop on *Pion and Kaon Structure at an Electron - Ion Collider*, 24–25 May 2018, The Catholic University of America, [www.jlab.org/conferences/pieic18/index.html].

[20] M. Burkardt, X.-d. Ji, and F. Yuan, Phys. Lett. **B545**, 345 (2002), arXiv:hep-ph/0205272 [hep-ph].

[21] X.-d. Ji, J.-P. Ma, and F. Yuan, Eur. Phys. J. **C33**, 75 (2004), arXiv:hep-ph/0304107 [hep-ph].

[22] C. Mezrag, H. Moutarde, and J. Rodriguez-Quintero, Few Body Syst. **57**, 729 (2016), arXiv:1602.07722 [nucl-th].

[23] C. Itzykson and J. B. Zuber, *Quantum Field Theory*, International Series In Pure and Applied Physics (McGraw-Hill, New York, 1980).

[24] D. Gromes, Z. Phys. **C57**, 631 (1993).

[25] C. H. Llewellyn-Smith, Annals Phys. **53**, 521 (1969).

[26] P. Maris and C. D. Roberts, Int. J. Mod. Phys. **E12**, 297 (2003), arXiv:nucl-th/0301049 [nucl-th].

[27] P. Maris and C. D. Roberts, Phys. Rev. **C56**, 3369 (1997), arXiv:nucl-th/9708029 [nucl-th].

[28] L. Chang and C. D. Roberts, Phys. Rev. **C85**, 052201 (2012), arXiv:1104.4821 [nucl-th].

[29] P. Maris and P. C. Tandy, Phys. Rev. **C60**, 055214 (1999), arXiv:nucl-th/9905056 [nucl-th].

[30] P. Maris and P. C. Tandy, Phys. Rev. **C62**, 055204 (2000), arXiv:nucl-th/0005015 [nucl-th].

[31] L. Chang, Y.-X. Liu, and C. D. Roberts, Phys. Rev. Lett. **106**, 072001 (2011), arXiv:1009.3458 [nucl-th].

[32] I. C. Cloët, W. Bentz, and A. W. Thomas, Phys. Lett. **B621**, 246 (2005), arXiv:hep-ph/0504229 [hep-ph].

[33] B. C. Tiburzi, W. Detmold, and G. A. Miller, Phys. Rev. **D68**, 073002 (2003), arXiv:hep-ph/0305190 [hep-ph].

[34] N. Souchlas, J. Phys. **G37**, 115001 (2010).

[35] G. P. Lepage and S. J. Brodsky, Phys. Rev. **D22**, 2157 (1980).

[36] G. R. Farrar and D. R. Jackson, Phys. Rev. Lett. **35**, 1416 (1975).

[37] X.-d. Ji, J.-P. Ma, and F. Yuan, Phys. Lett. **B610**, 247 (2005), arXiv:hep-ph/0411382 [hep-ph].

[38] S. J. Brodsky and F. Yuan, Phys. Rev. **D74**, 094018 (2006), arXiv:hep-ph/0610236 [hep-ph].

[39] P. J. Sutton, A. D. Martin, R. G. Roberts, and W. J. Stirling, Phys. Rev. **D45**, 2349 (1992).

[40] M. Gluck, E. Reya, and I. Schienbein, Eur. Phys. J. **C10**, 313 (1999), arXiv:hep-ph/9903288 [hep-ph].

[41] M. Botje, Comput. Phys. Commun. **182**, 490 (2011), arXiv:1005.1481 [hep-ph].

[42] A. Bacchetta, F. Delcarro, C. Pisano, M. Radici, and A. Signori, JHEP **06**, 081 (2017), arXiv:1703.10157 [hep-ph].

[43] A. Bacchetta, S. Cotogno, and B. Pasquini, Phys. Lett. **B771**, 546 (2017), arXiv:1703.07669 [hep-ph].

[44] H. Avakian, A. V. Efremov, P. Schweitzer, and F. Yuan, Phys. Rev. **D81**, 074035 (2010), arXiv:1001.5467 [hep-ph].

[45] D. Boer, L. Gamberg, B. Musch, and A. Prokudin, JHEP **10**, 021 (2011), arXiv:1107.5294 [hep-ph].

[46] J. Collins, Camb. Monogr. Part. Phys. Nucl. Phys. Cosmol. **32**, 1 (2011).

[47] S. M. Aybat and T. C. Rogers, Phys. Rev. **D83**, 114042 (2011), arXiv:1101.5057 [hep-ph].

[48] T. C. Rogers, Eur. Phys. J. **A52**, 153 (2016), arXiv:1509.04766 [hep-ph].

[49] J. S. Conway *et al.*, Phys. Rev. **D39**, 92 (1989).

[50] J. C. Collins and D. E. Soper, Nucl. Phys. **B197**, 446 (1982).

[51] X. Wang, Z. Lu, and I. Schmidt, JHEP **08**, 137 (2017), arXiv:1707.05207 [hep-ph].

[52] F. A. Ceccopieri, A. Courtoy, S. Noguera, and S. Scopetta, (2018), arXiv:1801.07682 [hep-ph].

[53] S. Arnold, A. Metz, and M. Schlegel, Phys. Rev. **D79**, 034005 (2009), arXiv:0809.2262 [hep-ph].

[54] I. Scimemi and A. Vladimirov, Eur. Phys. J. **C78**, 89 (2018), arXiv:1706.01473 [hep-ph].

[55] W. J. Stirling and M. R. Whalley, J. Phys. **G19**, D1 (1993).
[56] J. S. Ball and T.-W. Chiu, Phys. Rev. **D22**, 2542 (1980).
[57] J. S. Ball and T.-W. Chiu, Phys. Rev. **D22**, 2550 (1980), [Erratum: Phys. Rev.D23,3085(1981)].
[58] L. Chang, C. D. Roberts, and S. M. Schmidt, Phys. Rev. **C87**, 015203 (2013), arXiv:1207.5300 [nucl-th].
[59] L. Chang and C. D. Roberts, Phys. Rev. Lett. **103**, 081601 (2009), arXiv:0903.5461 [nucl-th].
[60] C. Shi, C. Mezrag, and H.-s. Zong, Phys. Rev. **D98**, 054029 (2018), arXiv:1806.10232 [nucl-th].